High-performance CO_2 Capture from Air by Harnessing the Power of CaO- and Superbase Ionic Liquid-Engineered Sorbents

Debabrata Moitra,[a] Narges Mokhtari-Nori,[a] Kevin M. Siniard,[a] Liqi Qiu,[a] Juntian Fan[a], Zhun Dong,[b] Wenda Hu,[c] Hongjun Liu,[d] De-en Jiang,[d] Hongfei Lin,[b] Jianzhi Hu,[c, e] Meijia Li,[f] Zhenzhen Yang,[f], * and Sheng Dai[a, f], *

[a] Dr. D. Moitra, N. Mokhtari-Nori, K. Siniard, Dr. L. Qiu, J. Fan, and Dr. S. Dai
Department of Chemistry, Institute for Advanced Materials and Manufacturing, University of Tennessee, Knoxville, TN 37996, USA
[b] Dr. Z. Dong and Dr. H. Lin
Voiland School of Chemical Engineering and Bioengineering, Washington State University, Pullman, Washington 99164, USA
[c] W. Hu and Dr. J. Hu
Pacific Northwest National Laboratory, Richland, Washington 99352, USA
[d] Dr. H. Liu, and Dr. D. Jiang
Department of Chemical and Biomolecular Engineering, Vanderbilt University, Nashville, TN 37235, USA
[e] Dr. J. Hu
Voiland School of Chemical Engineering and Bioengineering, Washington State University, Pullman, Washington 99164, USA
[f] Dr. M Li, Dr. Dr. Z. Yang, and Dr. S. Dai
Chemical Sciences Division, Oak Ridge National Laboratory, Oak Ridge, TN 37831, USA
E-mail: yangz3@ornl.gov; dais@ornl.gov
Supporting information for this article is given via a link at the end of the document.

Abstract: Direct air capture (DAC) of CO_2 by solid porous materials represents an attractive "negative emission" technology. However, state-of-the-art sorbents based on supported amines still suffer from unsolved high energy consumption and stability issues. Herein, taking clues from the CO_2 interaction with superbase-derived ionic liquids (SILs), high-performance and tunable sorbents in DAC of CO_2 was developed by harnessing the power of CaO- and SIL-engineered sorbents. Deploying mesoporous silica as the substrate, a thin CaO layer was first introduced to consume the surface-OH groups, and then active sites with different basicities (e.g., triazolate and imidazolate) were introduced as a uniformly distributed thin layer. The as-obtained sorbents displayed high CO_2 uptake capacity via volumetric (at 0.4 mbar) and breakthrough test (400 ppm CO_2 source), rapid interaction kinetics, facile CO_2 releasing, and stable sorption/desorption cycles. Operando Diffuse Reflectance Infrared Fourier Transformation Spectroscopy (DRIFTS) analysis under simulated air atmosphere and solid-state Nuclear Magnetic Resonance (NMR) under $^{13}CO_2$ atmosphere demonstrated the critical roles of the SIL species in low-concentration CO_2 capture. The fundamental insights obtained in this work provide guidance on the development of high-performance sorbents in DAC of CO_2 by leveraging the combined advantages of porous solid scaffolds and the unique features of CO_2-philic ILs.

Introduction

With the extensive consumption of fossil fuels and increasing demand for energy, the ever-increasing CO_2 content in the atmosphere is becoming an indisputably serious threat to global climatic balance.[1-8] According to a recent report published in 2021 by the Intergovernmental Panel on Climate Change (IPCC), by the end of this century, global warming could result in global temperatures increasing by 2 ºC[3, 9, 10] if large-scale "negative emission" (i.e., removal of CO_2 from ambient air) technologies are not deployed immediately.[11, 12] One of the most promising modes of such technology is to reduce the global atmospheric CO_2 concentration by capturing CO_2 directly from the air, which is known as Direct Air Capture (DAC).[3, 12-19] Nevertheless, capturing CO_2 from a very large volume of ambient air with low CO_2 concentrations (~ 400 ppm) remains challenging,[8, 20] and only limited sorbents have been developed for this purpose.

Liquid sorbents such as aqueous amine and alkaline hydroxide/carbonate solutions are state-of-the-art deployed systems in industrial applications, but still suffered from unsolved issues of volatility, equipment corrosion, inferior durability, and extensive energy consumption for cycling.[21-25] Solid sorbents via engineered chemisorption procedures could solve the solvent evaporation and corrosion issues to some extent, with most of the studies focused on amine-modified materials such as silica, carbon, metal-organic frameworks (MOFs), polymers, covalent organic frameworks (COFs), etc., taking clues from the reaction pathway of amines with CO_2.[13, 14, 16, 18, 20, 23, 26-28] In these materials, amines with diverse structures (e.g., primary, secondary, or tertiary types) are integrated into the porous supports via impregnation, covalent bond formation grafting through silylation reaction, or in situ polymerization using aziridines as monomers, generating sorbents capable of achieving DAC of CO_2 via C-N bond formation (Figure 1).[3, 13, 29] Notably, one of the strengths deploy solid sorbents in carbon capture is the diminished energy consumption for CO_2 releasing, as no extra energy input was required to heat the large volume of solvents. However, for the amine-modified solid sorbents in carbon capture, although the strong interaction strength with CO_2 via N-C bond formation (e.g., reaction enthalpy of -80 kJ mol^{-1})[4, 30, 31] could facilitate the efficient carbon capture from low-concentration sources, relatively high energy input is still required due to the limited tunability of these materials in terms of reaction energy with CO_2, as the CO_2-involved reaction still relies on the ammonium carbamate formation pathway in most cases.[3, 13] In addition, the amine-modified sorbents are prone to chemically and thermally degrade over time due to the inferior stability of amine moieties, and large hydrogen-bonding networks lead to inferior CO_2 sorption kinetics, especially in the presence of water-impurities.[4, 32] Although efforts have been made to solve these inadequacies by introducing anti-oxidation additives, deploying

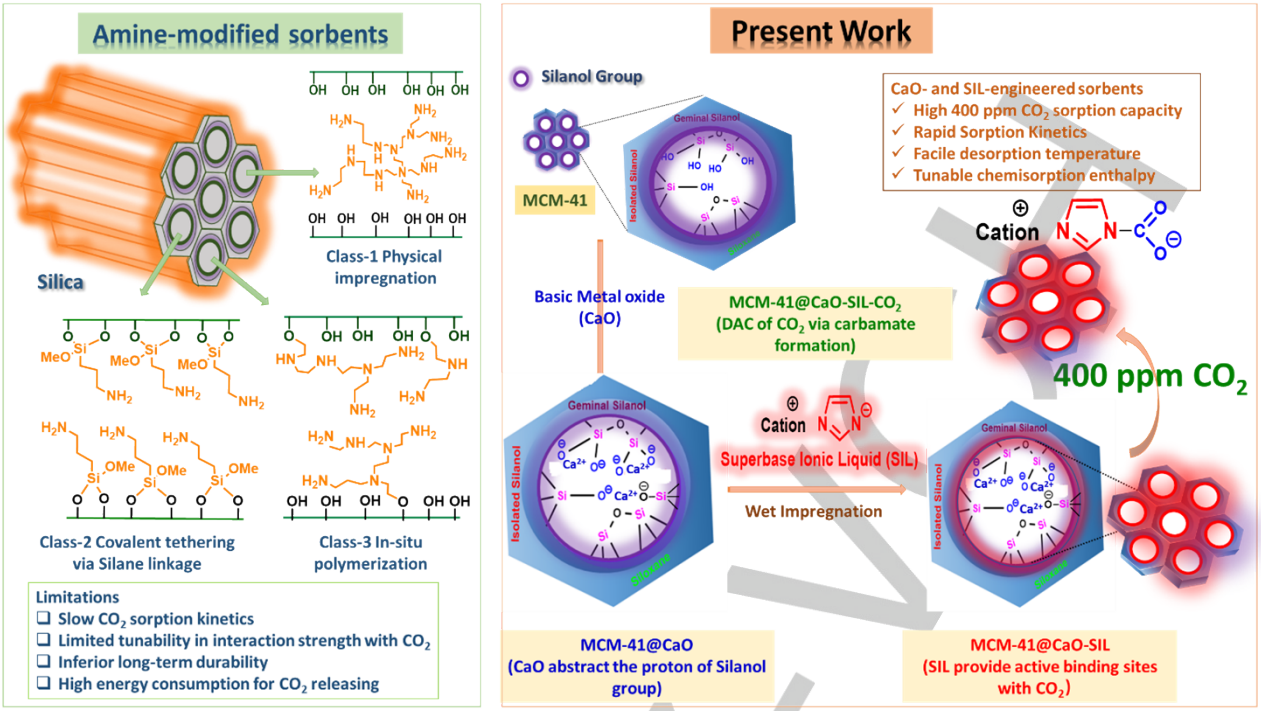

Figure 1. Schematic illustration and comparison of the previous reported amine-modified porous silica sorbents and the CaO- and SILs-engineered sorbents being developed in this work in the application of DAC via CO_2 chemisorption.

surface-modified supports, or utilizing branched amine precursors, the progress is still limited, and extra cost or tedious procedure is encountered in some techniques.[14, 33-37]

Notably, in the field of carbon capture via the chemisorption procedures, amino-based ionic liquids (AILs) have been demonstrated to solve the volatility and stability issues of amine solutions as liquid sorbents, through a similar reaction pathway to integrate CO_2 via C-N bond formation.[13, 20, 29] The unique features of ILs, including structure diversity, good stability, negligible volatility, and large tunability in the interaction strength with CO_2, has trigger extensive research efforts and the development of diverse functionalized ILs towards efficient carbon capture.[6, 38-41] Besides AILs, basic ILs with no active proton being involved in the structures, such as superbase-derived ILs (SILs), represent another category of functionalized ILs capable of achieving efficient CO_2 capture via C-N, C-O, or C-C bond formation.[8, 41-43] The fast carbon capture kinetics could be achieved by SILs without the extensive hydrogen-bonding network formation, together with the benefits from the low viscosity of SILs (as low as 8.63 cP in the absence of any solvents).[44] Notably, a sigmoid relationship between the reaction enthalpy and CO_2 uptake capacity of the ILs was demonstrated,[45] in which for a fixed CO_2-involved reaction pathway, a criterion enthalpy value existed to ensure the equilibrium (maximum theoretical) capacity being achieved and CO_2 releasing with minimum energy input, and reaction enthalpy surpassing this value have no contribution to the uptake capacity, but higher energy input was required for the desorption procedure. The reaction enthalpy of the SILs with could be facilely regulated by the structure and property (e.g., basicity) of the anions in a large region (e.g., from -19.1 to -90 kJ mol^{-1}), [4] making them promising candidates to act as modifiers to generate engineered solid sorbents for controllable DAC of CO_2 in terms of both high-performance carbon capture and energy-efficient carbon releasing. Notably, although the merits of SILs have been demonstrated in carbon capture procedures, the previous works are still focused on the pure CO_2 source or those containing high concentration CO_2 as the major components.[4, 41, 46-52] The unique nature of the DAC procedure will raise up new challenges and requirements on the design, synthesis, characterization, and sorption behaviour of the selected ILs-engineered solid sorbents to achieve high-performance DAC of CO_2 in practical applications. Therefore, alternative sorbents that combine the best attributes of solid sorbents and ILs possessing tunable reaction enthalpy, improved stability, high CO_2 uptake capacity from ambient air, fast carbon capture kinetics, and promising recyclability is still highly desired.

In this work, high performance and tunable DAC of CO_2 was achieved by harnessing the power of CaO- and SILs-bi-functionalized sorbents. The mesoporous silica MCM-41 supported was first coated by a thin layer of CaO films, which was then modified by selected SIL anions coupled with Na^+ cation. The volumetric CO_2 capture evaluation at 298 K revealed that CaO-modified MCM-41 (MCM-41@CaO (MSC)) exhibited reversible CO_2 capture behavior at low pressure region, possessing the CO_2 uptake capacity of 0.05 mmol g^{-1} at 0.4 mbar (close to 400 ppm), which was then further increased to 0.085 mmol g^{-1} and 0.125 mmol g-1 by further introducing the sodium triazolate (MSC-[Na][Triz]) and sodium imidazolate (MSC-[Na][Im]) coating, respectively. Additionally, fixed-bed breakthrough tests using ambient 400 ppm CO_2 concentrations demonstrated promising carbon capture behavior of MSC-[Na][Im] with a CO_2 uptake capacity of 0.91 mmol g^{-1} at 298 K, together with energy-efficient CO_2 releasing behavior and promising cycling stability within five cycles. The highly efficient, stable, and tunable 400 ppm CO_2 capture performance was demonstrated by SIL (phosphonium cation coupled with imidazolate anion)-functionalized MSC, taking

advantage of the reaction between imidazolate anion and CO_2. Operando Diffuse Reflectance Infrared Fourier Transformation Spectroscopy (DRIFTS) analysis under simulated air atmosphere and solid-state Nuclear Magnetic Resonance (NMR) under $^{13}CO_2$ atmosphere were conducted to provide more insights into the reaction mechanism and kinetics. The synthesis techniques and achievements made in this work represent the development of customized sorbents combining the unique features of nanoporous solid supports and SILs to deliver sorbents with high-performance DAC of CO_2, tunable reaction enthalpy, energy-efficient releasing, and robust cycling stability.

Results and Discussion

The porous silica supports have been widely deployed to produce high-performance solid sorbents towards DAC of CO_2 via diverse modification procedures leveraging their easy availability, robust and rigid architectures, permanent porous channels to facilitate mass transfer, and facile modification via the surface hydroxyl group-involved procedures.[9, 18, 50, 53] For example, amine-modified (e.g., polyethyleneimine (PEI), pentaethylenehexamine (PEHA), and tetraethylenepentamine (TEPA)) MCM-41 materials have been extensively studied in DAC of CO_2.[3, 16] Notably, for the synthesis of amine-modified sorbents, the surface hydroxyl groups of silica could act as reactive sites to construct covalent bonds (O-Si) for amine connections, or as hydrogen-bonding sites to stabilize the amino groups.[3] Comparatively, towards the introduction of SILs species within the porous channels of customized scaffolds, the residual hydroxyl groups have potential negative effect, which could deactivate the basic sites (generally anions) of the SILs via deprotonation. In addition, these hydroxyl groups are unfavorable to construct the hydrogen bonding formation-free sorbents for accelerated CO_2 sorption kinetics. Therefore, the pre-modification of the silica surface before SIL coating played a critical role in creating a suitable surface enabling good wettability for selected SIL and well maintenance of the active sites for CO_2 integration.

With all these considerations, herein, MCM-41 was deployed as the porous support precursor, the surface modification of which was first conducted by introducing a calcium oxide (CaO) layer (Figure 1). In fact, CaO itself has been deployed as sorbents for carbon capture generally at elevated temperatures.[10, 54, 55] Therefore, surface modification of MCM-41 by CaO will not only create a suitable surface for the subsequent SIL coating, but also benefit the CO_2 capture from air atmosphere via providing extra active sites. An in-situ decomposition technique was deployed to form the CaO using $Ca(OAC)_2$ as the precursor and calcium source, and the as-afforded material was denoted as MCM-41@CaO (MSC). For the selection of SILs, two types of anions, triazolate ($[Triz]^-$) and imidazolate ($[Im]^-$) with a CO_2 reaction enthalpy of -56.4 and -89.9 kJ mol^{-1} were deployed,[46, 56] with the former possessing weaker and the latter possessing similar interaction strength with CO_2 compared with amines. Both of them could react reversibly with CO_2 via C-N bond formation, producing carbamates as the product. In addition, to simplify the system and focus on the influence of the anions, the sodium salts, that is, [Na][Triz] and [Na][Im] (Figures S1-S4) was first deployed as the modifier to synthesize CaO and SIL-engineered MCM-41 towards DAC of CO_2 evaluation via the wet impregnation procedure, and the as-synthesized sorbents were denoted as MCM-41@CaO-[Na][Triz] (MSC--[Na][Triz]) and MCM-41@CaO-[Na][Im] (MSC-[Na][Im]), respectively (see SI for synthesis details).

The powder X-ray diffraction (PXRD) patterns of MCM-41 and MSC exhibited similar features with a broad peak representing the SiO_2 phase near $2\theta = 21^o$ (Figure S5), indicating the amorphous feature of the mesoporous silica scaffolds.[54, 57] In addition, no additional peaks were observed corresponding to the accumulation of big calcium oxide particles in MSC, confirming the successful incorporation of Ca ions within the lattice of silica in the form of a thin and uniform layer.[54] After further integration of the sodium salts, PXRD patterns of MSC-[Na][Triz] and MSC-[Na][Im] exhibited no obvious signals of the [Na][Triz] or [Na][Im] salts, indicating the uniformly disctributed sodium salt layer with no big particle accumulation (Figure S6).

The textural structure evolution upon the introduction of the CaO layer and sodium salt coating was evaluated by N_2 adsorption/desorption isotherms being collected at 77 K (Figure 2A and 2B and Table S1). The MCM-41 precursor exhibited a typical type IV isotherm demonstrating the presence of ordered mesoporous structures, with the Brunauer-Emmett-Teller (BET) surface area of 697 m^2 g^{-1}, total pore volume of 0.56 cm^3 g^{-1} mainly contributed by mesopores with the size around 3.9 nm. After CaO-engineering, the MSC exhibited diminished surface area (237 m^2 g^{-1}) but well-maintained mesoporous channels around 3.8 nm. Comparatively, further introducing the [Na][Im] coating layer led to further diminished surface area of 58 m^2 g^{-1}, and both micropores (1.9 nm) and mesopores (3.2 nm) still existed within the architecture. Notably, the N_2 isotherms (77 K) of MSC-[Na][Im] displayed combined features of type I and IV due to the existence of both micro- and mesopore. The rapid N_2 uptake at the low-pressure region ($P/P_0 < 0.05$) envisaged us to explore the possible existence of ultra-micropores in both MSC-[Na][Triz] and MSC-[Na][Im]. Accordingly, CO_2 possessing smaller kinetic diameter (3.3 Å) than N_2 (3.64 Å) was deployed as the probe molecular, and the CO_2 adsorption/desorption isotherms were collected at 195 K to provide related information (Figure S7).[58] The surface area of MSC-[Na][Triz] and MSC-[Na][Im] was calculated to be 103 and 115 cm^3 g^{-1}, respectively, together with ultra-micropores located around 0.6 nm within the architectures.

To understand the interaction between the -[Na][Im] and the surface of MCM-41 modified with CaO, the FTIR spectra of MCM-41, MSC and MSC-[Na][Im] was acquired (Figure 2C). Based on the FTIR evaluations of MCM-41, an intense band at approximately 3384 cm^{-1} is observed and assigned to the -OH stretches of the surface silanols. The peak at 1639 cm^{-1} indicates the Si-OH deformational vibrations of adsorbed molecules. The band at 1019 cm^{-1}, with a corresponding shoulder at 1226 cm^{-1} and a band at 776 cm^{-1}, are assigned to the internal and external asymmetric Si-O stretching modes.[59-61] In the FTIR spectra of MSC, no significant changes were observed in the lower energy region of the FTIR spectrum, indicating MSC has similar skeleton as that of MCM-41. However, the absence of corresponding peak of -OH and Si-OH at 3384 cm^{-1} and 1639 cm^{-1}, respectively, in MSC indicates the existence of strong interaction between the basic CaO sites with the surface -OH groups of MCM-41. Similar results were observed after impregnation of [Na][Triz] or [Na][Im] in MSC in the higher energy region of FTIR spectra. However, some additional characteristic peaks are observed due to the introduction of imidazolate functional groups at 1650 cm^{-1}, 1505

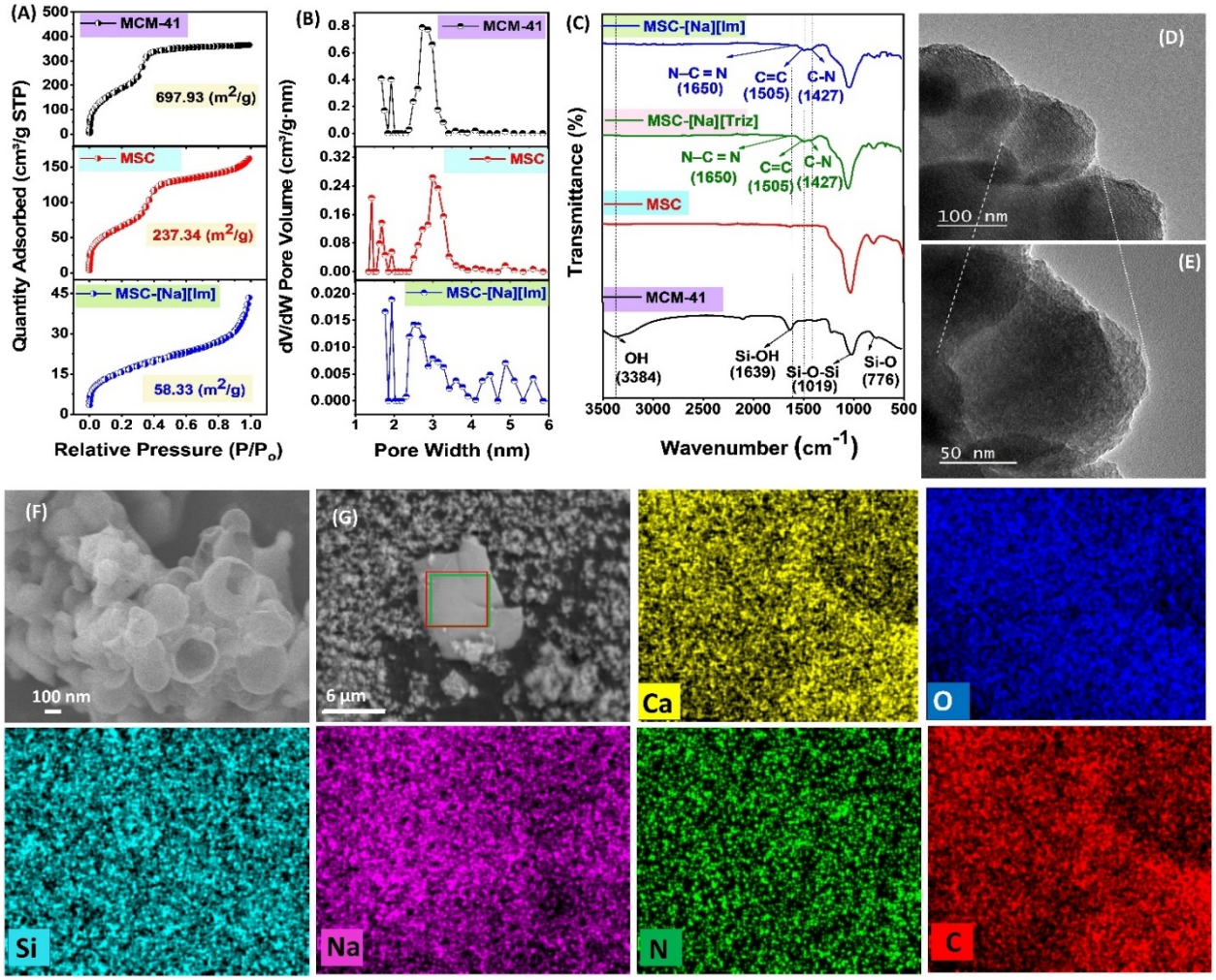

Figure 2 Characterizations of MCM-41, MSC, and MSC-[Na][Im]. (A) N_2 adsorption-desorption isotherm curves, (B) pore size distribution curves being calculated by the non-local density functional theory (NL-DFT) method, (C) FTIR spectra of MCM-41, MSC, and MSC-[Na][Im]. (D-E) TEM micrographs of MSC-[Na][Im]. (F) SEM Image of MSC-[Na][Im] (G) Elemental mapping of the synthesized MSC-[Na][Im] composite.

cm^{-1} and 1427 cm^{-1} belonging to N-C=N, C=C and C-N of imidazolate ring, respectively.[62, 63]

The morphology of the obtained materials was assessed by high-resolution transmission electron microscopy (TEM) and scanning electron microscopy (SEM) analysis. The TEM micrograph of pure MCM-41, MSC and MSC-[Na][Im] composites are shown in Figure S8A, Figure S8B, and Figure 2D and 2E respectively. TEM of the parent sample plainly showed some key features of MCM-41 (Figure S8A). The silica microspheres displayed a pseudo-periodic lattice of a parallel bundle of pores. The TEM image of MSC sample shown in Figure S8B presented a similar pore shape related to the pure MCM-41 sample. However, partially irregular pore-ordering and morphological defects were observed which were probably related to a partial collapse of the structure of MCM-41 due to the high loading amount of CaO (20 wt%). Figure 2D and 2E showed the TEM images of MSC-[Na][Im], which clearly indicated the retention of porous structure in the composite after impregnation of [Na][Im] species.

The SEM micrographs of MCM-41 (Figure S8C) and MSC (Figure S8D) clearly show the structure of silica with a spherical shape. However, smaller spheres and irregular agates of amorphous silica being stuck to larger spheres can be observed in the morphology of MSC after calcium oxide loading (Figure S8D). The SEM image of MSC-[Na][Im] (Figure 2F) revealed that the morphology of the support precursor was well retained. Elemental mapping of MSC-[Na][Im] composites is shown in Figure 2G, which indicates the presence and homogeneous distribution of Ca, Si, Na, O, N, and C elements in these composites. Energy dispersive X-ray (EDX) analysis of MCM-41, MSC and MSC-[Na][Im] are shown in Figure S9. EDX analysis of MCM-41 indicates the presence of Si and O (Figure S9A). After CaO loading, MSC shows the presence of Ca, Si, and O (Figure S9B). Upon coating with [Na][Im], MSC-[Na][Im] features Ca, Si, Na, O, N, and C signals (Figure S9C) alluding to the successful integration of [Na][Im] with MSC for enhanced CO_2 adsorption. The thermal stability of the synthesized MSC-[Na][Im] was investigated by thermogravimetric analysis (TGA) under nitrogen atmosphere (Figure S10). Based on TGA analysis, the composite began to lose weight at about 150 ºC with maximum weight loss occurring at 200 ºC, which represents the complete decomposition of the sodium salt. The undecomposed residue of ~ 80 % is due to the leftover MSC.

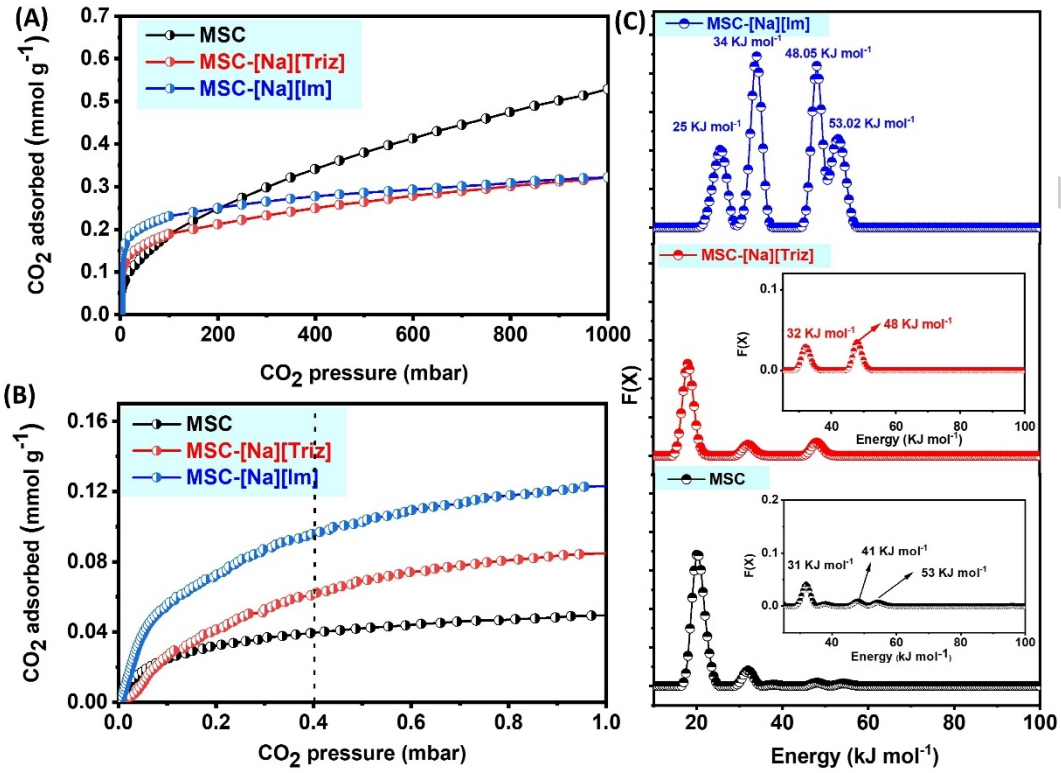

Figure 3 (A-B) CO_2 uptake isotherms within different pressure regions being collected at 298 K. (C) The energy distribution curves for CO_2 interaction with MSC, MSC-[Na][Triz] and MSC-[Na][Im].

To understand the process of the carbon capture behavior, the CO_2 uptake isotherms of MSC, MSC-[Na][Triz] and, MSC-[Na][Im] were first studied and compared by a volumetric method with CO_2 pressure set up to 1000 mbar at 298 K (Figure 3A and 3B). It can be clearly observed that the CO_2 uptake capacity of MSC at ambient pressure (0.53 mmol g^{-1}) surpassed that being obtained by MSC-[Na][Im] (0.32 mmol g^{-1}) and MSC-[Na][Triz] (0.31 mmol g^{-1}), mainly caused by the different surface areas. The rapid CO_2 uptake at low pressure region was observed when MSC was further modified by [Na][Im] and [Na][Triz]. Particularly, the CO_2 uptake capacity being achieved by MSC-[Na][Triz] and MSC-[Na][Im] surpassed the MSC at the pressure region lower than 100 and 1 mbar, respectively, benefiting from the strong interaction strength of the sorbent surface with CO_2 endowed by the [Na][Triz] and [Na][Im] layers. A detailed evaluation in the CO_2 pressure region below 1 mbar further demonstrated the significant enhancement induced by the basic heterocyclic anion modification. At the CO_2 pressure of 0.4 mbar (close to 400 ppm), the CO_2 uptake capacity exhibited the following trend: MSC-[Na][Im] (0.125 mmol g^{-1}) > MSC-[Na][Triz] (0.085 mmol g^{-1}) > MSC (0.050 mmol g^{-1}) (Figure 3B), which was mainly affected by the basicity of the active sites, demonstrating the promising performance of the MSC-[Na][Im] composites in DAC of CO_2.

Furthermore, the sorption energy distribution curves between CO_2 and different MCM-41-based sorbents were calculated using the CAESAR (computed adsorption/absorption energies, singular value decomposition (SVD) analysis result) algorithm based on the CO_2 uptake isotherms (298 K) via MATLAB.[56, 64, 65] It is evident from Figure 3C that corresponding to the physisorption of CO_2, a major peak at the interaction energy of 20 kJ mol^{-1} was displayed in MSC, together with three minor peaks at 31, 41, and 53 kJ mol^{-1} indicating the presence of chemisorption active sites. Comparatively, in the energy distribution diagrams of MSC-[Na][Triz], the peak at 32 and 48 kJ mol^{-1} became more significant, indicating the increased ratios of strong CO_2 binding sites. Notably, for MSC-[Na][Im], the chemisorption peaks located at 34, 48, and 53 kJ mol^{-1} even surpassed the physisorption one at 25 kJ mol^{-1}, which was preferred in low-concentration CO_2 uptake. This provides guidance on how to determine the distribution and ratio of physisorption and chemisorption sites possessing different interaction energy with CO_2 within the porous architectures. It also indicates that those containing strong chemisorption CO_2 sites have the potential to absorb low-concentration CO_2.[42] Moreover, the design of DAC sorbents with tunable chemisorption capability can significantly reduce the energy consumption of the DAC process.

Subsequently, a fixed bed breakthrough experiment was conducted at 298 K to further study the carbon capture behavior with 400 ppm CO_2 as the feeding gas (Figure S11). Since the highest uptake capacity of CO_2 at 0.4 mbar (close to 400 ppm) was observed for MSC-[Na][Im] composite via the volumetric method, it was chosen as a suitable material for further evaluation. A fixed-bed reactor was custom-built to perform breakthrough experiments. The background collection was first conducted with an empty bed to determine the mean residence time of the gas steam through the fixed bed. The background CO_2 breakthrough curve is shown by the black solid line in Figure 4A along with the measured CO_2 breakthrough curves for the CO_2 uptake capacity of MSC-[Na][Im]. Breakthrough and pseudo equilibrium capacities were calculated based on the measured breakthrough curves at 5% and 95 % of C_0 (inlet CO_2 concentration) respectively and are

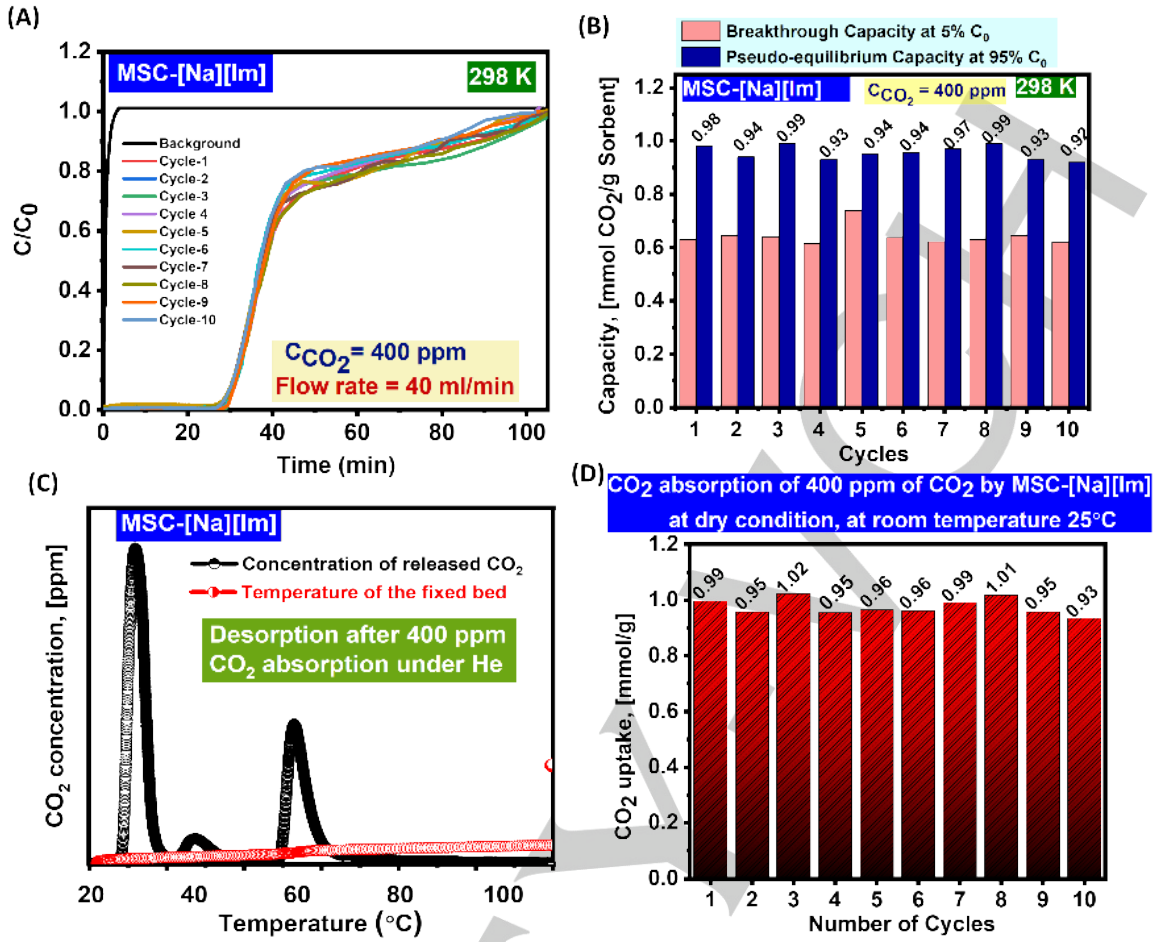

Figure 4 (A) The breakthrough curves for MSC-[Na][Im] being collected at 298 K featuring ten cycles with 400 ppm CO_2 in He as the feeding source. (B) Breakthrough (C/C_o = 0.05) and pseudo equilibrium (C/C_o = 0.95) CO_2 capture capacities of MSC-[Na][Im] for up to ten cycles. (C) CO_2 TPD profile of 400 ppm CO_2 saturated MSC-[Na][Im]. (D) The equilibrium CO_2 uptake capacities of MSC-[Na][Im] for up to ten cycles CO_2 releasing was performed under the He gas flow (90 mL min^{-1}) at 353 K for 60 min.

shown in Figure 4B where up to 10 cycles are featured. It was observed from the breakthrough experiment that at 298 K, the CO_2 uptake capacity of MSC-[Na][Im] reaches a maximum value of ~1.02 mmol g^{-1} (Figure 4A). The pseudo-equilibrium capacity and the breakthrough capacity are calculated to be ~0.97 and ~0.63 mmol g^{-1} respectively and are consistent up to 10 cycles. The temperature-programmed desorption (TPD) experiments were conducted for MSC-[Na][Im] sorbent to gain better insights into the CO_2 releasing behavior (Figure 4C). It is well evident that the entire desorption process takes place at a temperature range of 25 – 70 ºC with three distinguished peaks indicating the CO_2 desorption from three types of active sorption sites at 30, 40, and 62 ºC, respectively. Therefore, it was demonstrated that the chemisorbed CO_2 by MSC-[Na][Im] could be released under mild conditions with much less energy input compared to the amine-modified sorbents.[13] The stability and the performance of the developed MSC-[Na][Im] sorbents were analyzed by performing CO_2 adsorption-desorption tests for up to five consecutive cycles. It was observed that the breakthrough times for ten cycles were almost identical (Figure 4A), alluding to great recyclability of the material. Based on the breakthrough curves, in the tenth cycle, 95% of the equilibrium capacity of MSC-[Na][Im] was still maintained (0.95 mmol/g). (Figure 4D). Furthermore, to quantitively characterize the adsorption kinetics behavior of the fixed-bed column, we have kinetically modeled breakthrough curves of MSC-[Na][Im] using the computational fluid dynamics method (see SI for the details). The experimental uptake isotherm shown in Figure. 3A is far from equilibrium due to a short contact time between CO_2 and sorbents. Hence, we used the pseudo-equilibrium capacity ~0.97 mmol/g obtained from the breakthrough experiment of MSC-[Na][Im] as an approximation of q_e at 0.4 mbar. The Toth fitting (n_s = 0.17 mmol/g, b = 7.8 $mbar^{-1}$, t_T=0.66) was scaled accordingly to represent the whole equilibrium isotherm in Figure S12A. We showed the homogeneous kinetic model cannot properly capture the prolonged tails observed in experimental breakthrough curves (see Figure S12B). To overcome this deficiency, we applied a heterogeneous kinetic model and found a reasonable agreement of breakthrough curves between model prediction and experiment shown in Figure S12C. The modeled CO_2 adsorbed amount on sorbents as a function of time is shown in Figure S12D. The predicted breakthrough time of 30 min, breakthrough capacity of 0.61 mmol/g and pseudo-equilibrium capacity of 0.95 mmol/g agree satisfactorily with experimental values.

The influence of different coating amounts of CaO and [Na][Im], as well as the comparison between the [Na][Im] and

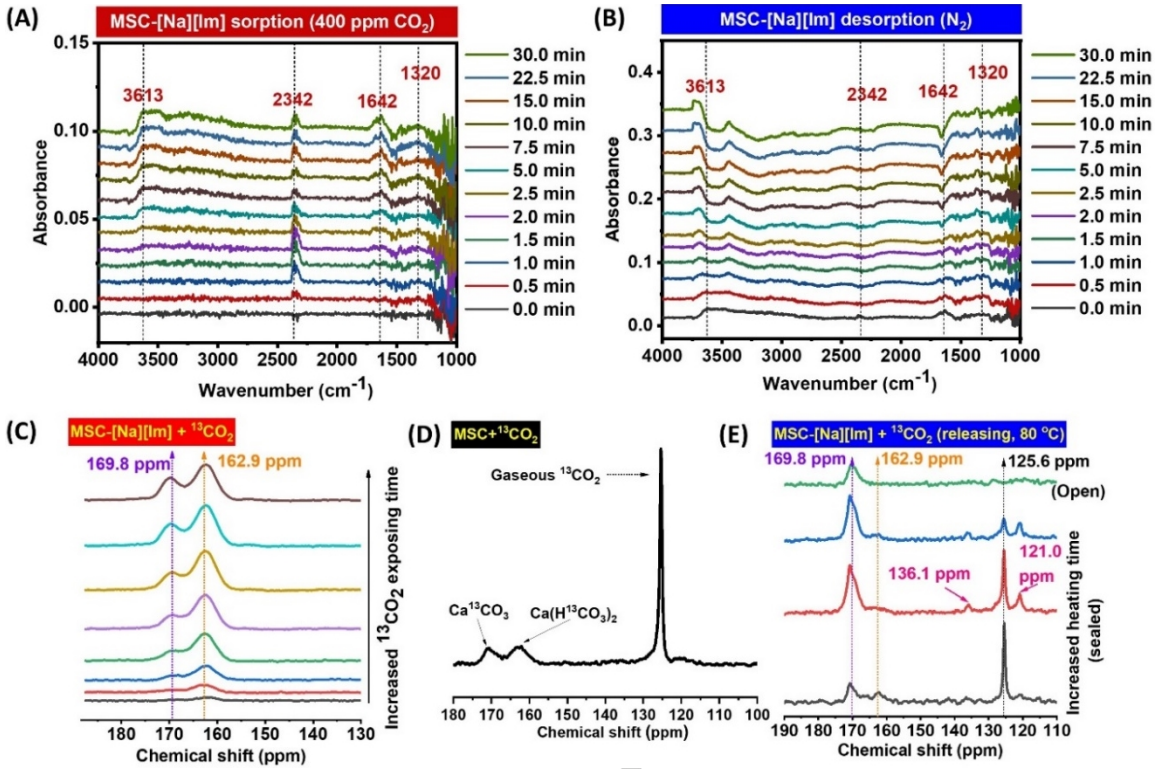

Figure 5 (A) In situ DRIFTS spectra of MSC-[Na][Im] under air atmosphere with 400 ppm CO_2 being involved. (B) The corresponding desorption spectra being collected at 353 K under nitrogen atmosphere. (C) The in situ ^{13}C CP/MAS NMR spectra of MSC-[Na][Im] upon exposing to $^{13}CO_2$ (15 psi) at 298 K. (D) ^{13}C NMR spectrum of MSC after reacting with $^{13}CO_2$. (E) CO_2 releasing behavior of $^{13}CO_2$-saturated MSC-[Na][Im] at the heating temperature of 353 K.

[Na][Triz] layer introduction, on the (400 ppm) CO_2 uptake capacity was then studied via the breakthrough test (Figure S12). First, when MCM41 without CaO modification was deployed as the support, MCM41-[Na][Im] exhibited inferior CO_2 uptake capacity (0.0613 mmol g^{-1}) due to the deactivation of imidazolate sites by the -OH groups on the surface, illustrating the critical role of the CaO layer introduction to achieve high-performance DAC of CO_2 (Figure S12A). Notably, for MSC and MSC-[Na][Im], 20 wt% Ca precursor and 20 wt% [Na][Im] was added in the sorbent synthesis, which could be also denoted as MSC-20, and MSC-20-[Na][Im]-20, respectively. For the MSC-10 sorbent being obtained using half amount of the Ca precursor, a CO_2 uptake capacity of 0.085 mmol g^{-1} was obtained (Figure S12B), which was much lower than the corresponding [Na][Im]-involved sorbent, indicating that the low-concentration CO_2 uptake within MSC-10-[Na][Im]-20 (0.17 mmol g^{-1}) was mainly contributed by the basic imidazolate sites (Figure S12C). In addition, the coating amount of CaO played critical roles to ensure the high-performance CO_2 uptake. It was noted that MSC-10-[Na][Im]-20 displayed lower CO_2 capacity than MSC-20-[Na][Im]-20 (0.91 mmol g^{-1}). It was probably due to insufficient neutralization of the surface -OH groups by CaO, which in turn deactivated the imidazolate sites. The CO_2 uptake capacity of MSC10-NaTriz20 and MSC20-NaTriz20 was measured to be 0.15 mmol g^{-1} (Figure S12D) and 0.19 mmol g^{-1} respectively (Figure S12E), illustrating the benefits of [Na][Im] coating with stronger basicity than [Na][Triz]. Notably, further increasing the coating amount of [Na][Im] from 20 wt.% in MSC to 30 wt.% and 50 wt.%, respectively, with the sorbents being denoted as MSC-20-[Na][Im]-30 and MSC-20-[Na][Im]-50, the opposite CO_2 uptake capacity trend was demonstrated in the trend of MSC-20-[Na][Im]-20 (0.91 mmol g^{-1}) > MSC-20-[Na][Im]-30 (0.42 mmol g^{-1}) (Figure S12F) > MSC-20-[Na][Im]-50 (0.24 mmol g^{-1}) (Figure S12G). The inferior influence of excess amount of [Na][Im] coating in the carbon capture behavior may be caused by the pore blocking effect, which led to slow CO_2 sorption kinetics, illustrating the critical role on the thin [Na][Im] layer formation on the pore walls. After the CO_2 chemisorption by the outer layer of [Na][Im], no more CO_2 could penetrate the inner NaIm compositions due to the dense phase of the [Na][Im] layer.

Furthermore, to gain a deep insight into the reaction pathway and sorption kinetics, operando diffuse reflectance infrared Fourier transform spectroscopy (DRIFTS) analysis under air atmosphere (400 ppm CO_2) was performed. Taking the IR spectrum of MSC-[Na][Im] as the background, upon exposing to the air atmosphere at 298 K, three new peaks located at 1642, 1320 cm^{-1} and 3613 cm^{-1} are immediately observed after 1.5 min (Figure 5A), the intensity of which was gradually increased by prolonging the collection time and kept constant after 30 min, demonstrating the fast CO_2 sorption kinetics (Figure S13). The peaks at 1642 and 1320 cm^{-1} can be attributed to the stretching vibrations of C=O and N-COO^- skeletal vibration of carbamate, respectively.[49, 66, 67] The peak at 3613 cm^{-1} appeared due to the formation of overtones of the gas phase CO_2.[66, 68] The peak at 2342 cm^{-1} is assigned to physiosorbed CO_2.[66] The results indicated that the carbamate was formed between the basic nitrogen sites of imidazolate anion and CO_2. Subsequently, the CO_2 releasing procedure was also monitored under nitrogen atmosphere by raising the temperature to 353 K (Figure 5B). Complete disappearance of the characteristic peaks for bonded CO_2 (1642 and 1320 cm^{-1}), as well as the physically adsorbed ones (2342 cm^{-1}), was observed within 5 min. Therefore, the operando

DRIFTS demonstrated that CO_2 was captured mainly via C-N bond formation between the imidazolate moiety and CO_2. Subsequently, the operando solid-state ^{13}C cross-polarization magic-angle spinning ^{13}C nuclear magnetic resonance (CP/MAS ^{13}C NMR) analysis was performed to detect species with restricted molecular motion, i.e., the chemisorbed CO_2, the carbons in solid state and at solid surfaces adopting $^{13}CO_2$ as the feeding source. It was noted that when 15 psi $^{13}CO_2$ was charged to the MSC-[Na][Im], two distinct peaks at 169.8 ppm, and 162.9 ppm were observed (Figure 5C). The peak at 162.9 ppm is assigned to generation of carbamate product via N-C bond formation between imidazolate anion and $^{13}CO_2$.[46] Notably, the 169.8 ppm peak polarize slower, indicating it is more remote from protons compared with the 162.9 ppm peak, which may be generated from the interaction of $^{13}CO_2$ with the MSC support. To gain more insights, the operando ^{13}C NMR of MSC support was collected upon interacting with CO_2 (Figure 5D). Besides the gaseous $^{13}CO_2$, a major peak located at 169.8 ppm together with a shoulder at 161.8 ppm was observed, which was caused by the formation of $Ca^{13}CO_3$ and $Ca(H^{13}CO_3)_2$, respectively, with the proton being provided by the surface –Si-OH groups for the formation of bicarbonate species. Therefore, when MSC-[Na][Im] was deployed as the sorbent to react with CO_2, both carbamate and carbonate products were obtained via the reaction of CO_2 with imidazolate and CaO, respectively. The $^{13}CO_2$ releasing behavior was then studied at 80 °C (Figure 5E). The carbamate product (162.9 ppm) was decomposed gradually to release $^{13}CO_2$ even under sealed environment, which completely disappeared when the rotor was open, indicating that heating at 80 °C could enable the complete releasing of the $^{13}CO_2$ being captured by the imidazolate layer. However, the as-formed $Ca^{13}CO_3$ (169.8 ppm) was still maintained after heating treatment over the opened rotor, considering its high decomposition temperature (> 450 °C). No residual $Ca(H^{13}CO_3)_2$ was shown up after the heating treatment, which may decompose to $Ca^{13}CO_3$ (169.8 ppm). Notably, when the released CO_2 was in a confined environment, transient states with two peaks located at 136.1 and 121.0 ppm were observed, which was probably the intermediate states between free $^{13}CO_2$ molecules and the N-C bond formation towards the carbamate salts. It should be pointed out that although $Ca^{13}CO_3$ formation was observed under pure CO_2 atmosphere, this may not be the case when 400 ppm CO_2 was deployed as the gas source. The operando NMR studies confirmed that upon exposing the MSC-[Na][Im] to CO_2 atmosphere, the imidazolate anion is first involved in CO_2 capture and the procedure is reversible to enable the energy-efficient CO_2 releasing and sorbent cycling.

With the promising results displayed by the introduction of [Na][Im] coating in carbon capture from air, the corresponding SIL composed of tetrabutylphosphonium cation and imidazolate anion, $[P_{4444}][Im]$, was deployed to modify MSC, and the sorbent was denoted as MSC--$[P_{4444}][Im]$ (Figure S14 and Figure S15). The carbon capture behavior of which was then detailly studied by volumetric and breakthrough methods (Figure 6). The carbon capture by MSC--$[P_{4444}]$ [Im] was first measured by volumetric method with CO_2 pressure up to 1000 mbar at 298 K (Figure 6A and 6B). It was observed that the CO_2 uptake capacity of MSC-$[P_{4444}]$ [Im] at ambient pressure and at the CO_2 pressure of 0.4 mbar (close to 400 ppm) was found to be 0.225 and 0.062 mmol g^{-1}, respectively. The rapid increase of CO_2 uptake capacity by MSC--$[P_{4444}]$ [Im] at low pressure region indicates the formation of a thin layer of SIL coating on the surface of MSC and introduction of strong CO_2 reactive sites (imidazolate anions). Hence, to

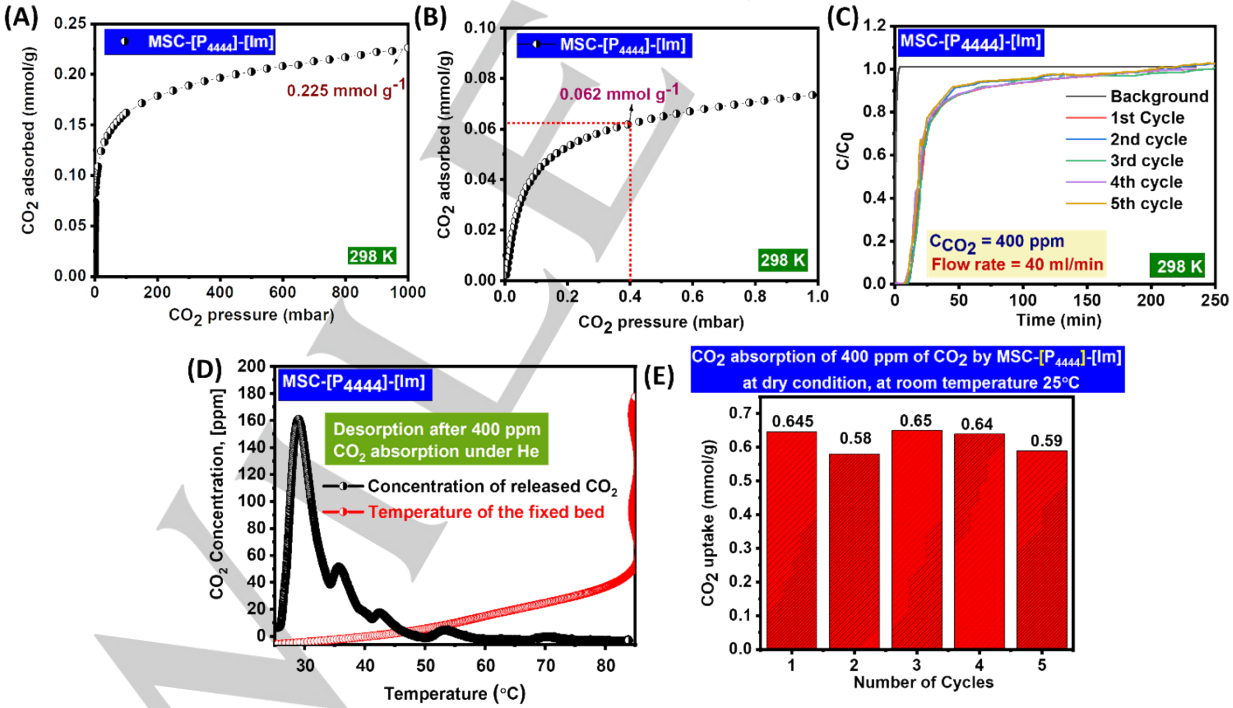

Figure 6 (A-B) CO_2 uptake isotherms within different pressure regions being collected at 298 K (C) The breakthrough curves for MSC-$[P_{4444}]$ [Im] being collected at 298 K featuring five cycles with 400 ppm CO_2 in He as the feeding source. (D) CO_2 TPD profile of MSC-$[P_{4444}]$ [Im] under He atmosphere. (E) The equilibrium CO_2 uptake capacities of MSC-$[P_{4444}]$ [Im] for up to five cycles. CO_2 releasing was performed under the He gas flow (90 mL min^{-1}) at 353 K for 60 min.

demonstrate the potential application of MSC-$[P_{4444}]$ [Im] towards DAC, the breakthrough experiment was conducted at 298 K to further study the carbon capture behavior with 400 ppm CO_2 as the feeding gas (Figure 6C). It was observed from the

breakthrough experiment that at 298 K, the CO_2 uptake capacity of -[P_{4444}] [Im]-56 reaches a maximum value of ~0.65 mmol g^{-1} (Figure 6C) and is consistent up to 5 cycles. The temperature-programmed desorption (TPD) experiments were conducted for MSC--[P_{4444}] [Im] sorbent to gain better insights into the CO_2 releasing behavior (Figure 6D). It is well evident that the entire desorption process takes place at a temperature range of 25 – 80 ºC with five distinguished peaks at 30, 37, 45, 58 and 78 ºC. Therefore, it was demonstrated that the chemisorbed CO_2 by MSC--[P_{4444}] [Im] could be released under mild conditions with much less energy input compared to the amine-modified sorbents. The stability and the performance of the developed sorbents were then analyzed by performing CO_2 adsorption-desorption cycle tests for up to five consecutive cycles. Based on the breakthrough curves, MSC--[P_{4444}] [Im] maintained stable capacities of ~0.64 mmol g^{-1} for the five consecutive cycles. It should be noted that compared with the amine-based systems, the scalability and cost of the SIL-derived systems are still inferior currently, and the related studies are mainly under fundamental stage. However, the large-scale applications of ILs have been demonstrated in biomass-involved procedures, with the cost lower than regular organic solvents.[69] Therefore, considering the merits of SIL-derived systems, particularly the non-volatility, long-term stability, and large-tuning capability, they are promising sorbents for practical DAC applications.

Conclusion

In this work, efforts have been made to construct functionalized sorbents towards efficient DAC of CO_2 via structure engineering. MCM41 was deployed as the substrate, which was first modified by a thin layer of CaO to consume the surface -OH groups. Subsequently, taking the clues in CO_2 capture by SIL, active and basic anions, i.e., triazolate and imidazolate, were introduced aiming at capturing CO_2 from low-concentration sources. Volumetric CO_2 uptake and the corresponding breakthrough test demonstrated the rapid CO_2 uptake and high CO_2 uptake capacity being achieved by CaO- and [Na][Im]-bifunctionalized sorbents, together with low energy consumption for CO_2 releasing (at 353 K) good cycling stability. Reaction pathway studies were conducted via DRIFTS under air atmosphere and operando ^{13}C NMR test with $^{13}CO_2$ as the feeding source, both illustrating the benefits of the imidazolate anion introduction in DAC of CO_2 via the N-C bond formation and carbamate product generation, as well as the facile releasing of the captured CO_2 and good reversibility of the sorption/desorption procedure. Then, a SIL was deployed to coat the surface of MSC and the as-formed sorbents displayed promising application in DAC of CO_2, achieving high CO_2 uptake capacity at 0.4 mbar pressure or from 400 ppm CO_2 in He, easy CO_2 releasing under mild conditions, and stable CO_2 uptake performance within repeated cycles. The fundamental insights being obtained in this work provide guidance on the development of high-performance sorbents in DAC of CO_2 by leveraging the combined advantages of porous solid scaffolds and the unique features of CO_2-philic ILs.

Acknowledgements

The research was supported financially by the Division of Chemical Sciences, Geosciences, and Biosciences, Office of Basic Energy Sciences, US Department of Energy (Award No. DE-SC0022273).

Keywords: Carbon dioxide, Carbon capture, Direct Air Capture, Superbase-derived ionic liquids, Chemisorption behavior

Reference

[1] R. K. Pachauri, M. R. Allen, V. R. Barros, J. Broome, W. Cramer, R. Christ, J. A. Church, L. Clarke, Q. Dahe, P. Dasgupta, *Climate change 2014: synthesis report. Contribution of Working Groups I, II and III to the fifth assessment report of the Intergovernmental Panel on Climate Change*, IPCC, **2014**.
[2] M. J. Lashaki, S. Khiavi, A. Sayari, *Chem. Soc. Rev.* **2019**, *48*, 3320-3405.
[3] E. S. Sanz-Pérez, C. R. Murdock, S. A. Didas, C. W. Jones, *Chem. Rev.* **2016**, *116*, 11840-11876.
[4] J. Ren, L. Wu, B.-G. Li, *Ind. Eng. Chem. Res.* **2013**, *52*, 8565-8570.
[5] R. Monastersky, *Nature* **2013**, *497*, 13-15.
[6] S. Zeng, X. Zhang, L. Bai, X. Zhang, H. Wang, J. Wang, D. Bao, M. Li, X. Liu, S. Zhang, *Chem. Rev.* **2017**, *117*, 9625-9673.
[7] K. Sumida, D. L. Rogow, J. A. Mason, T. M. McDonald, E. D. Bloch, Z. R. Herm, T.-H. Bae, J. R. Long, *Chem. Rev.* **2012**, *112*, 724-781.
[8] Z. Yang, S. Dai, *Green Chem. Eng.* **2021**, *2*, 342-345.
[9] R. Kumar, M. Bandyopadhyay, M. Pandey, N. Tsunoji, *Microporous Mesoporous Mater.* **2022**, *338*, 111956.
[10] C. Gunathilake, M. Jaroniec, *J. Mater. Chem. A* **2016**, *4*, 10914-10924.
[11] F. M. Brethomé, N. J. Williams, C. A. Seipp, M. K. Kidder, R. Custelcean, *Nat. Energy* **2018**, *3*, 553-559.
[12] P. Boone, Y. He, A. R. Lieber, J. A. Steckel, N. L. Rosi, K. M. Hornbostel, C. E. Wilmer, *Nanoscale* **2022**, *14*, 16085-16096.
[13] X. Shi, H. Xiao, H. Azarabadi, J. Song, X. Wu, X. Chen, K. S. Lackner, *Angew. Chem. Int. Ed.* **2020**, *59*, 6984-7006.
[14] S. A. Didas, S. Choi, W. Chaikittisilp, C. W. Jones, *Acc. Chem. Res.* **2015**, *48*, 2680-2687.
[15] G. Rim, F. Kong, M. Song, C. Rosu, P. Priyadarshini, R. P. Lively, C. W. Jones, *JACS Au* **2022**, *2*, 380-393.
[16] A. Sayari, Q. Liu, P. Mishra, *ChemSusChem* **2016**, *9*, 2796-2803.
[17] K. Lackner, H.-J. Ziock, P. Grimes, Los Alamos National Lab.(LANL), Los Alamos, NM (United States), **1999**.
[18] A. Cherevotan, J. Raj, S. C. Peter, *J. Mater. Chem. A* **2021**, *9*, 27271-27303.
[19] A. Kumar, D. G. Madden, M. Lusi, K. J. Chen, E. A. Daniels, T. Curtin, J. J. Perry IV, M. J. Zaworotko, *Angew. Chem. Int. Ed.* **2015**, *54*, 14372-14377.
[20] M. A. Alkhabbaz, P. Bollini, G. S. Foo, C. Sievers, C. W. Jones, *J. Am. Chem. Soc.* **2014**, *136*, 13170-13173.
[21] R. Custelcean, *Chem. Sci.* **2021**, *12*, 12518-12528.
[22] J. K. Stolaroff, D. W. Keith, G. V. Lowry, *Environ. Sci. Technol.* **2008**, *42*, 2728-2735.
[23] A. Sayari, Y. Belmabkhout, *J. Am. Chem. Soc.* **2010**, *132*, 6312-6314.
[24] D. W. Keith, G. Holmes, D. S. Angelo, K. Heidel, *Joule* **2018**, *2*, 1573-1594.
[25] F. S. Zeman, K. S. Lackner, *World Resource Review* **2004**, *16*, 157-172.
[26] S. Himeno, T. Komatsu, S. Fujita, *Adsorption* **2005**, *11*, 899-904.
[27] L. Zhou, J. Wu, M. Li, Q. Wu, Y. Zhou, *Chem. Eng. Sci.* **2005**, *60*, 2833-2844.
[28] A. Goeppert, M. Czaun, R. B. May, G. S. Prakash, G. A. Olah, S. Narayanan, *J. Am. Chem. Soc.* **2011**, *133*, 20164-20167.
[29] J. Septavaux, C. Tosi, P. Jame, C. Nervi, R. Gobetto, J. Leclaire, *Nat. Chemy* **2020**, *12*, 202-212.
[30] I. Kim, H. F. Svendsen, *Ind. Eng. Chem. Res.* **2007**, *46*, 5803-5809.
[31] N. McCann, M. Maeder, M. Attalla, *Ind. Eng. Chem. Res.* **2008**, *47*, 2002-2009.

[32] K. E. Gutowski, E. J. Maginn, *J. Am. Chem. Soc.* **2008**, *130*, 14690-14704.

[33] X. Zhu, W. Xie, J. Wu, Y. Miao, C. Xiang, C. Chen, B. Ge, Z. Gan, F. Yang, M. Zhang, *Chem. Soc. Rev.* **2022**.

[34] T. Wang, K. S. Lackner, A. B. Wright, *Phys. Chem. Chem. Phys.* **2013**, *15*, 504-514.

[35] R. Hughes, G. Kotamreddy, A. Ostace, D. Bhattacharyya, R. L. Siegelman, S. T. Parker, S. A. Didas, J. R. Long, B. Omell, M. Matuszewski, *Energy Fuels* **2021**, *35*, 6040-6055.

[36] B. Dinakar, A. C. Forse, H. Z. Jiang, Z. Zhu, J.-H. Lee, E. J. Kim, S. T. Parker, C. J. Pollak, R. L. Siegelman, P. J. Milner, *J. Am. Chem. Soc.* **2021**, *143*, 15258-15270.

[37] P.-Q. Liao, X.-W. Chen, S.-Y. Liu, X.-Y. Li, Y.-T. Xu, M. Tang, Z. Rui, H. Ji, J.-P. Zhang, X.-M. Chen, *Chem. Sci.* **2016**, *7*, 6528-6533.

[38] S. Sarmad, J. P. Mikkola, X. Ji, *ChemSusChem* **2017**, *10*, 324-352.

[39] M. Watanabe, M. L. Thomas, S. Zhang, K. Ueno, T. Yasuda, K. Dokko, *Chem. Rev.* **2017**, *117*, 7190-7239.

[40] G. Gebresilassie Eshetu, M. Armand, B. Scrosati, S. Passerini, *Angew. Chem. Int. Ed.* **2014**, *53*, 13342-13359.

[41] S. Zheng, S. Zeng, Y. Li, L. Bai, Y. Bai, X. Zhang, X. Liang, S. Zhang, *AIChE J.* **2022**, *68*, e17500.

[42] X. Suo, Y. Fu, C.-L. Do-Thanh, L.-Q. Qiu, D.-e. Jiang, S. M. Mahurin, Z. Yang, S. Dai, *J. Am. Chem. Soc.* **2022**, *144*, 21658-21663.

[43] Y. Fu, X. Suo, Z. Yang, S. Dai, D.-e. Jiang, *J. Phys. Chem. B* **2022**, *126*, 6979-6984.

[44] C. Wang, H. Luo, D. e. Jiang, H. Li, S. Dai, *Angew. Chem.* **2010**, *122*, 6114-6117.

[45] K. Huang, Y.-T. Wu, S. Dai, *Ind. Eng. Chem. Res.* **2015**, *54*, 10126-10133.

[46] C. Wang, X. Luo, H. Luo, D. e. Jiang, H. Li, S. Dai, *Angew. Chem.* **2011**, *21*, 5020-5024.

[47] C. Wang, H. Luo, X. Luo, H. Li, S. Dai, *Green Chem.* **2010**, *12*, 2019-2023.

[48] J. F. Brennecke, B. E. Gurkan, *J. Phys. Chem. Lett.* **2010**, *1*, 3459-3464.

[49] C.-P. Ye, R.-N. Wang, X. Gao, W.-Y. Li, *Energy Fuels* **2020**, *34*, 14379-14387.

[50] M. Mohamedali, H. Ibrahim, A. Henni, *Microporous Mesoporous Mater.* **2020**, *294*, 109916.

[51] J. Cheng, Y. Li, L. Hu, J. Liu, J. Zhou, K. Cen, *Fuel Process. Technol.* **2018**, *172*, 216-224.

[52] J. Cheng, Y. Li, L. Hu, J. Zhou, K. Cen, *Energy Fuels* **2016**, *30*, 3251-3256.

[53] B. Lee, Z. Ma, Z. Zhang, C. Park, S. Dai, *Microporous Mesoporous Mater.* **2009**, *122*, 160-167.

[54] N. Pal, T. Kim, J.-S. Park, E.-B. Cho, *RSC Adv.* **2018**, *8*, 35294-35305.

[55] R. Chang, X. Wu, O. Cheung, W. Liu, *J. Mater. Chem. A* **2022**, *10*, 1682-1705.

[56] N. Mokhtari‐Nori, H. Luo, R. Paul, F. Vautard, Y. Fu, J. Fan, D. e. Jiang, Z. Yang, S. Dai, *Chem.Nano.Mat.* **2022**, e202200480.

[57] J. Tu, R. Wang, W. Geng, X. Lai, T. Zhang, N. Li, N. Yue, X. Li, *Sens. and Actuators B: Chem.* **2009**, *136*, 392-398.

[58] S. Du, J. Huang, M. R. Ryder, L. L. Daemen, C. Yang, H. Zhang, P. Yin, Y. Lai, J. Xiao, S. Dai, *Nat. Commun.* **2023**, *14*, 1197.

[59] E. A. Paukshtis, M. A. Yaranova, I. S. Batueva, B. S. Bal'zhinimaev, *Microporous and Mesoporous Mater.* **2019**, *288*, 109582.

[60] C. G. Okoye-Chine, C. O. L. Mbuya, T. S. Ntelane, M. Moyo, D. Hildebrandt, *J. Catal.* **2020**, *381*, 121-129.

[61] Z. Alirezvani, M. G. Dekamin, E. Valiey, *ACS Omega* **2019**, *4*, 20618-20633.

[62] S. S. Abolmaali, A. Tamaddon, H. Najafi, R. Dinarvand, *J. Inorg. Organomet. Polym. Mater.* **2014**, *24*, 977-987.

[63] M. Mahmoodi, A. Behzad‐Behbahani, S. Sharifzadeh, S. S. Abolmaali, A. Tamaddon, *IET nanobiotechnol.* **2017**, *11*, 995-1004.

[64] K. M. Nelson, S. M. Mahurin, R. T. Mayes, B. Williamson, C. M. Teague, A. J. Binder, L. Baggetto, G. M. Veith, S. Dai, *Microporous and Mesoporous Mater.* **2016**, *222*, 94-103.

[65] P. J. Dauenhauer, O. A. Abdelrahman, *ACS Cent. Sci.* **2018**, *4*, 1235-1243.

[66] S. Chakravartula Srivatsa, S. Bhattacharya, *J. CO_2 Util.* **2018**, *26*, 397-407.

[67] C. S. Srikanth, S. S. Chuang, *J. Phys. Chem. C* **2013**, *117*, 9196-9205.

[68] Y. Hu, Z. Liu, J. Xu, Y. Huang, Y. Song, *J. Am. Chem. Soc.* **2013**, *135*, 9287-9290.

[69] C. Li, D. Tanjore, W. He, J. Wong, J. L. Gardner, K. L. Sale, B. A. Simmons, S. Singh, *Biotechnol. Biofuels* 2013, *6*, 1-13.

Entry for the Table of Contents

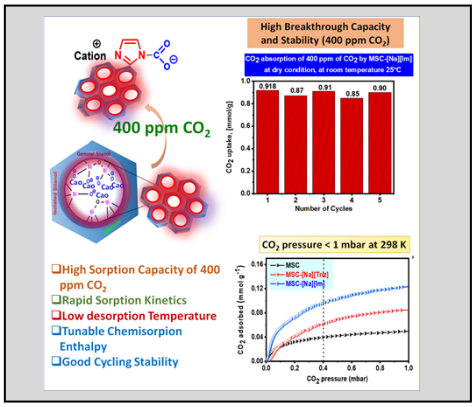

High-performance direct air capture of CO_2 has been demonstrated by CaO- and superbase-derived ionic liquids (SIL)-bifunctionalized sorbents. By leveraging the combined merits of porous solid sorbents and the unique features of SIL, high CO_2 uptake capacity via volumetric (at 0.4 mbar) and breakthrough test (400 ppm CO_2 source), rapid interaction kinetics, facile CO_2 releasing, and stable sorption/desorption cycles were achieved, together with detailed reaction mechanism studies via operando FTIR and NMR techniques.